 Human Molecular Genetics, 2000, Vol. 9, No. 12 **1865–1871**

Identification of two new *Pmp22* mouse mutants using large-scale mutagenesis and a novel rapid mapping strategy

Adrian M. Isaacs, Kay E. Davies, A. Jackie Hunter[1], Patrick M. Nolan[2], Lucie Vizor[2], Jo Peters[2], Davina G. Gale[3], David P. Kelsell[4], Ian D. Latham[3], Jennifer M. Chase[3], Elizabeth M.C. Fisher[5], Mark M. Bouzyk[3], Allyson Potter, Mohan Masih, Frank S. Walsh[1], Matthew A. Sims[3], Kim E. Doncaster[3], Claire A. Parsons[3], Jo Martin[6], Steven D.M. Brown[2], Sohaila Rastan[3], Nigel K. Spurr[3] and Ian C. Gray[3,+]

Department of Human Anatomy and Genetics, University of Oxford, Oxford OX1 3QX, UK, [1]Department of Neuroscience, SmithKline Beecham Pharmaceuticals, New Frontiers Science Park, Harlow, Essex CM19 5AW, UK, [2]MRC Mammalian Genetics Unit and UK Mouse Genome Centre, Harwell, Oxon OX11 ORD, UK, [3]Department of Biotechnology and Genetics, SmithKline Beecham Pharmaceuticals, New Frontiers Science Park, Harlow, Essex CM19 5AW, UK, [4]Centre for Cutaneous Research, Queen Mary and Westfield College, London E1 4NS, UK, [5]Department of Neurogenetics, Imperial College, London SW7 2AZ, UK and [6]Department of Histopathology, Queen Mary and Westfield College, London E1 4NS, UK

Received 7 April 2000; Revised and Accepted 29 May 2000

Mouse mutants have a key role in discerning mammalian gene function and modelling human disease; however, at present mutants exist for only 1–2% of all mouse genes. In order to address this phenotype gap, we have embarked on a genome-wide, phenotype-driven, large-scale *N*-ethyl-*N*-nitrosourea (ENU) mutagenesis screen for dominant mutations of clinical and pharmacological interest in the mouse. Here we describe the identification of two similar neurological phenotypes and determination of the underlying mutations using a novel rapid mapping strategy incorporating speed back-crosses and high throughput genotyping. Two mutant mice were identified with marked resting tremor and further characterized using the SHIRPA behavioural and functional assessment protocol. Back-cross animals were generated using *in vitro* fertilization and genome scans performed utilizing DNA pools derived from multiple mutant mice. Both mutants were mapped to a region on chromosome 11 containing the peripheral myelin protein 22 gene (*Pmp22*). Sequence analysis revealed novel point mutations in *Pmp22* in both lines. The first mutation, H12R, alters the same amino acid as in the severe human peripheral neuropathy Dejerine Sottas syndrome and Y153TER in the other mutant truncates the Pmp22 protein by seven amino acids. Histological analysis of both lines revealed hypomyelination of peripheral nerves. This is the first report of the generation of a clinically relevant neurological mutant and its rapid genetic characterization from a large-scale mutagenesis screen for dominant phenotypes in the mouse, and validates the use of large-scale screens to generate desired clinical phenotypes in mice.

INTRODUCTION

As the sequencing phase of the Human Genome Project nears completion, the need for new approaches to tackle gene function analysis in a mammalian system is abundantly clear. Large-scale mutagenesis in the mouse is set to offer a solution to this requirement by providing a comprehensive resource of mouse mutants linking gene with phenotype. We have recently initiated a large-scale *N*-ethyl-*N*-nitrosurea (ENU) mutagenesis project in the mouse for this purpose (1).

ENU has been shown to be a potent mutagen in the mouse (2) that creates mainly point mutations; a male mouse injected with ENU can produce many mutant offspring. A screen for dominant phenotypes allows mutants to be identified in the first generation of progeny of an injected male. To identify and characterize mutant phenotypes generated from our mutagenesis programme, the SHIRPA [SmithKline Beecham Pharmaceuticals, Harwell MRC Mouse Genome Centre and Mammalian Genetics Unit, Imperial College School of Medicine (St Mary's) Royal London Hospital, St Bartholomew's and the Royal London School of Medicine Phenotype Assessment] protocol, a wide-ranging and sensitive screen for mouse mutants (3), is used. If a phenotype is shown to be stably inherited, the gene involved can then be positionally cloned.

[+]To whom correspondence should be addressed. Tel: +44 1279 627225; Fax: +44 1279 622500; Email: ian_gray-1@sbphrd.com

The ability to rapidly identify the underlying genetic mutation will be crucial to the success of large-scale mutagenesis programmes as functional genomics tools. We have identified mutations in two mouse mutants generated from our programme using a mapping strategy involving *in vitro* fertilization (IVF) to quickly produce sufficient numbers of back-cross mice followed by pooling of the mouse DNA to facilitate a rapid genome scan.

Large-scale mutagenesis will be an important tool for generating better mouse models of human diseases. This phenotype-driven approach will produce models that closely resemble human disorders without any assumptions concerning the genes involved. This should allow new biological pathways involved in disease aetiology and pathogenesis to be uncovered. The mutants described here, trembler-m1H (Tr-m1H) and trembler-m2H (Tr-m2H), two mice with a clinically relevant resting tremor phenotype, are shown to have mutations in the peripheral myelin protein 22 (*Pmp22*) gene. Pmp22 is a constituent of peripheral nerve myelin, and mutations in human *PMP22* can cause the peripheral neuropathies Charcot–Marie–Tooth disease (CMT), Dejerine Sottas syndrome (DSS) and hereditary neuropathy with liability to pressure palsies (HNPP) (4). The characterization of new mutations in *Pmp22* indicates the potential of large-scale mutagenesis screens for developing animal models of human disease.

RESULTS

Tr-m1H and Tr-m2H phenotype

Tr-m1H and Tr-m2H were identified from the progeny of two separate male BALB/c mice injected with ENU and mated with C3H/HeH females. Both mice exhibited a marked resting tremor and were smaller than littermates at weaning, remaining so into adulthood. Tr-m1H was more severely affected, having fits and a more marked tremor. Mutant lines were established by back-crossing both mutants to C3H/HeH, and the SHIRPA protocol (3) used to more fully assess the behavioural and functional phenotype of each mutant (Table 1). Both lines were inactive, showed low locomotor activity and had abnormal gaits with low body position and splayed legs. Both lines failed the wire manoeuvre, an indicator of truncal and limb strength and also performed poorly on an accelerating rotarod, an indicator of motor coordination (5), on which Tr-m1H showed a greater deficit. Both had defects in grip strength, with Tr-m1H again more severely affected. On tail suspension, both exhibited limb grasping, with Tr-m1H exhibiting a particularly vigorous extension and flexion of the hind limbs. No sensory deficit was evident, all digits were normal and the toe pinch response was unimpaired. These results indicate some impairment of muscle or motor function and provide a semi-quantitative measure of the difference in severity of the phenotypes of Tr-m1H and Tr-m2H.

Table 1. SHIRPA data for parameters that differed between Tr-m1H, Tr-m2H and controls

Parameter	Score			
	Range	Littermate controls (n = 8)	Tr-m2H (n = 5)	Tr-m1H (n = 4)
Body position[a]	0–5	3	2	2
Tremor[b]	0–2	0	2	2
Transfer arousal[c]	0–6	3	2	2
Locomotor activity[d]	*n*	2.9	1.8	1.5
Gait[e]	0–3	0	1–2	2
Limb grasp[f]	0–1	0	1	1
Grip strength[g]	0–4	2	1	0–1
Wire manoeuvre[h]	0–4	0	3	3
Skin colour[i]	0–2	1	0–1	0
Righting reflex[j]	0–3	0	1	2

[a]0, completely flat; 1, lying on side; 2, lying prone; 3, sitting or standing; 4, rearing on hind legs; 5, repeated vertical leaping.
[b]0, none; 1, mild; 2, marked.
[c]0, coma; 1, prolonged freeze, then slight movement; 2, extended freeze, then moderate movement; 3, brief freeze (few seconds), then active movement; 4, momentary freeze, then swift movement; 5, no freeze, immediate movement; 6, extremely excited (manic).
[d]Number of 11 cm^2 squares entered by all four feet in 30 s.
[e]0, normal; 1, fluid but abnormal; 2, limited movement only; 3, incapacity.
[f]0, absent; 1, present.
[g]0, none; 1, slight grip, semi-effective; 2, moderate grip, effective; 3, active grip, effective; 4, unusually effective.
[h]The mice were held above the wire by tail suspension and lowered to allow the forelimbs to grip the horizontal wire, they were then held in extension and rotated around to the horizontal and released. 0, active grip with hindlegs; 1, difficulty to grasp with hindlegs; 2, unable to grasp with hindlegs; 3, unable to lift hindlegs, falls within seconds; 4, falls immediately.
[i]Colour gradations of plantar surface and digits of forelimbs. 0, blanched; 1, pink; 2, bright, deep red flush.
[j]The mice were held by the tail and flicked backwards through the air such that they performed a backward somersault when released. 0, lands on feet (no impairment); 1, lands on side; 2, lands on back; 3, fails to right when placed on back.

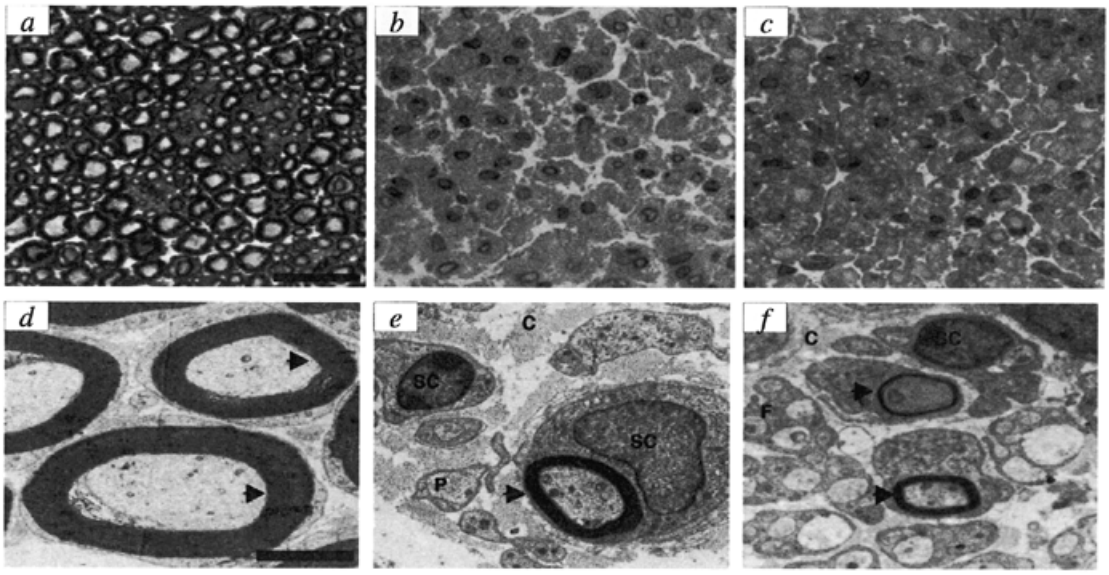

Figure 1. Light (a–c) and electron (d–f) microscope histology of sciatic nerve from 8-week-old mice. (**a**) Tr-m1H littermate control. Axons are surrounded by darkly staining myelin sheaths. (**b**) Tr-m2H. Schwann cell nuclei stain darkly and are enlarged and increased in numbers. There are few myelin sheaths, a reduction in the number of axonal profiles, and an increase in the amount of endoneurial connective tissue. (**c**) Tr-m1H shows similar pathology to Tr-m2H, with even fewer myelin sheaths. (**d**) Tr-m1H littermate control. (**e**) Tr-m2H. (**f**) Tr-m1H. The axons and surrounding myelin sheaths are greatly reduced in size compared with the control. The myelin sheaths present in Tr-m1H are thinner than those in Tr-m2H and surround axons of smaller diameter. F, fetal myelin, an early stage of myelin development, when many axons are associated with a single Schwann cell; P, promyelin, a later stage of myelin development, just prior to the formation of the myelin sheath, in which one axon is associated with one Schwann cell; C, collagen granules; S, Schwann cell nuclei, which are enlarged in Tr-m2H and Tr-m1H. Arrowheads indicate myelin sheaths. The scale bar in (a) is 20 μm, (a)–(c) are the same size; the scale bar in (d) is 2 μm, (d)–(f) are the same size.

Hypomyelination of Tr-m1H and Tr-m2H peripheral nerve

Histopathological analysis of Tr-m1H and Tr-m2H showed the morphology of the brain and spinal cord to be normal and Luxol fast blue staining revealed no gross loss of central nervous system myelin (data not shown). Peripheral nerves were examined by light and electron microscopy (Fig. 1). Hypomyelination was apparent in both lines, the few myelin sheaths present were thin and surrounded axons of small diameter. There was a decrease in the number of axonal profiles and an increase in the amount of endoneurial connective tissue. The number and size of Schwann cell nuclei was also increased. The pathology of Tr-m1H was more severe than that of Tr-m2H, having fewer, generally thinner myelin sheaths, mirroring the severity of the phenotype.

Tr-m1H and Tr-m2H map between *D11Mit131* and *D11Mit177*

IVF (6) of C3H/HeH eggs with sperm from Tr-m1H and Tr-m2H mice was used to speed the generation of a significant number of back-cross progeny. The resulting offspring were scored for the tremor phenotype and an autosomal dominant inheritance pattern with complete penetrance confirmed in each case. Equimolar aliquots of DNA from Tr-m1H (n = 45) or Tr-m2H (n = 44) mutant back-cross mice were combined, and duplicate DNA pools scanned with 229 CA repeat markers multiplexed into 23 panels, spanning the mouse genome with an average spacing of 10 cM. By measuring the peak heights of fluorescently labelled alleles using a modified version of TrueAllele genotyping software (7), we compared BALB/c:C3H/HeH allele ratios in each DNA pool. The expected signal ratio for the two alleles of an unlinked marker is 1 BALB/c:3 C3H/HeH in back-cross mice. As a recombination fraction of zero between the mutant gene and marker is approached, the signal ratio approaches 1:1 (Fig. 2). Differential amplification of BALB/c and C3H/HeH alleles was accounted for by comparison with individual F_1 heterozygote genotypes and appropriate adjustment of signal strength. Linkage for both Tr-m1H and Tr-m2H was detected on chromosome 11, with the minimal region bounded by markers *D11Mit131* and *D11Mit177*. Genotyping of individual mice confirmed the pooled data and identified recombinants between the mutant phenotype and *D11Mit131* [25.1 cM from the centromere (8)] and *D11Mit177* [35.0 cM from the centromere (8)], thus defining a 9.9 cM minimal interval (Fig. 3). No recombinants were identified with intervening marker *D11Mit242* (31.7 cM). *Pmp22* lies 30.6 cM from the centromere (9).

Tr-m1H and Tr-m2H have mutations in *Pmp22*

The genomic structure of *Pmp22* was determined by direct bacterial artificial clone (BAC) clone sequencing across exon–intron junctions using the human *PMP22* gene structure (10) to predict splice sites. *Pmp22* exons 2–5 (exon 1 is non-coding) were PCR amplified and sequenced from three mutant back-cross mice from each tremor strain together with the parental

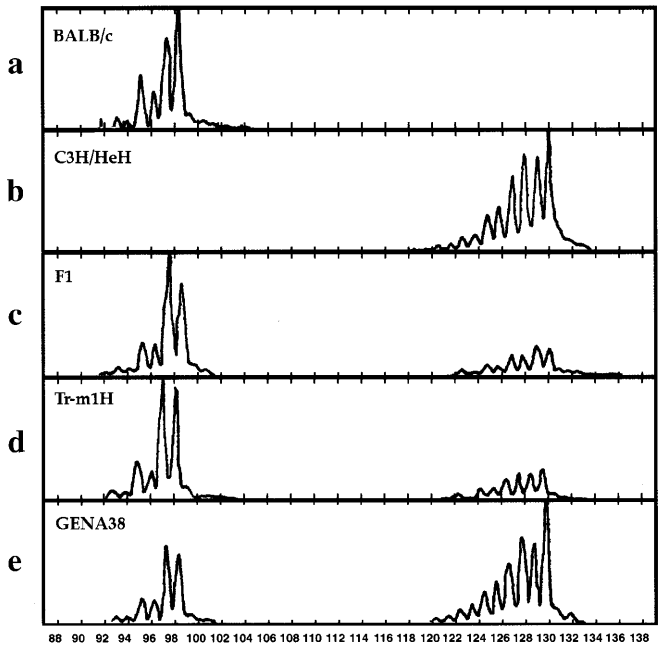

Figure 2. Linkage of the Tr-m1H phenotype to microsatellite marker *D11Mit242*. (**a**) Parental BALB/c marker profile. The trace profile represents a single 98 bp allele (additional peaks are observed before the main peak due to polymerase slippage and terminal transferase activity). (**b**) Parental C3H/HeH marker profile representing a single 130 bp allele. (**c**) BALB/c × C3H/HeH F_1 profile showing both BALB/c- and C3H/HeH-derived alleles. Note preferential amplification of the shorter 98 bp allele. (**d**) Tr-m1H mutant back-cross pooled DNA profile ($n = 45$). The allele peak height ratio is almost identical to that for the F_1 shown in (c), suggesting 1 BALB/c allele:1 C3H/HeH allele and linkage of *D11Mit242* to the Tr-m1H phenotype. (**e**) Pooled DNA from back-cross GENA38 mice ($n = 44$). The GENA38 phenotype, a negative control not linked to *D11Mit242* shows the expected 1 BALB/c:3 C3H/HeH peak height ratio after correction for preferential amplification of the shorter BALB/c allele.

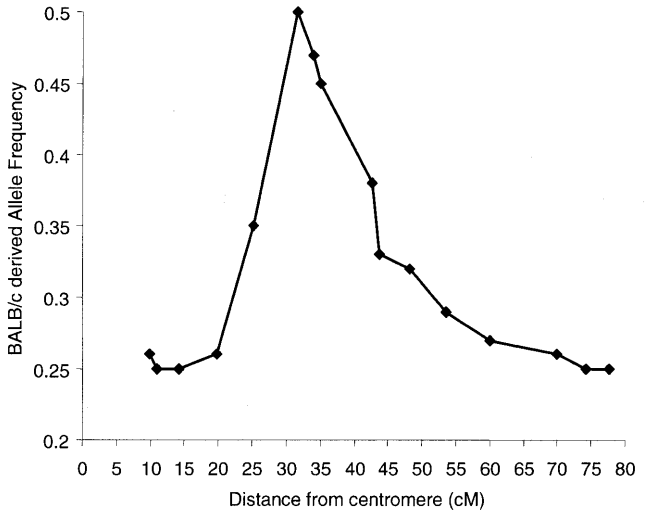

Figure 3. Frequency of BALB/c-derived alleles for mouse chromosome 11 markers in 45 Tr-m1H mutant back-cross mice. The expected frequency of the BALB/c-derived allele for a marker not linked to the Tr-m1H phenotype is 0.25. The BALB/c allele frequency increases for linked markers; as the recombination fraction approaches zero, the frequency of the BALB/c-derived allele approaches 0.5. No recombinants were observed for marker *D11Mit242* (31.7 cM from the centromere). Recombinants were observed for the flanking markers *D11Mit131* (25.1 cM) and *D11Mit177* (35.0 cM), defining a 9.9 cM critical interval.

BALB/c and C3H/HeH strains. An A→G transition in codon 12 resulting in a His→Arg amino acid substitution was identified in all Tr-m1H mutant mice (Fig. 4). A His→Gln mutation has been identified at this site in an individual suffering DSS (11), a demyelinating neuropathy similar to (but more severe than) CMT type 1 (CMT1), which also results from *PMP22* point mutations in some cases (4). Tr-m1H may therefore prove a more accurate mouse model for DSS than those currently available. An A→T transversion in codon 153 resulting in a premature stop codon truncating the Pmp22 protein by seven amino acids was identified in all Tr-m2H mutant mice (Fig. 4). The truncation removes the last three amino acids of the fourth transmembrane domain and final four amino acids of the intracellular C-terminal domain. Parental strains had wild-type alleles at both positions implying that both mutations were a result of ENU administration. Both mutations are different from the three previously identified spontaneous *Pmp22* mouse mutants (12–14) (Table 2) and are the only *Pmp22* mutants on a common genetic background.

Table 2. Mouse *Pmp22* mutants

Mutant allele	Mutation[a]	Background strain	Reference
$Pmp22^{Tr}$	G^{449}→A (G150D)	Outbred	13
$Pmp22^{Tr\text{-}J}$	T^{47}→C (L16P)	C57BL/6J	14
$Pmp22^{Tr\text{-}Ncnp}$	In-frame deletion of exon 4	GAD/Ncnp	15
$Pmp22^{Tr\text{-}m1H}$	A^{35}→G (H12R)	BALB/c	–
$Pmp22^{Tr\text{-}m2H}$	T^{459}→A (Y153TER)	BALB/c	–

[a]The position of the mutation within the coding sequence is given in superscript and the corresponding amino acid change in parentheses.

DISCUSSION

PMP22 alterations are responsible for a significant proportion of cases of dominantly inherited hereditary peripheral neuropathy. CMT1 is the most common form of hereditary peripheral neuropathy and its largest subtype, CMT type 1A (CMT1A), is caused by either a 1.5 Mb duplication of a region of chromosome 17p11.2 that contains *PMP22*, or *PMP22* point mutations (4). DSS, which is characterized by an early age of onset and a more severe phenotype than CMT1A, can also be caused by point mutations in *PMP22* (4). This varying degree of severity in human peripheral neuropathies associated with *PMP22*

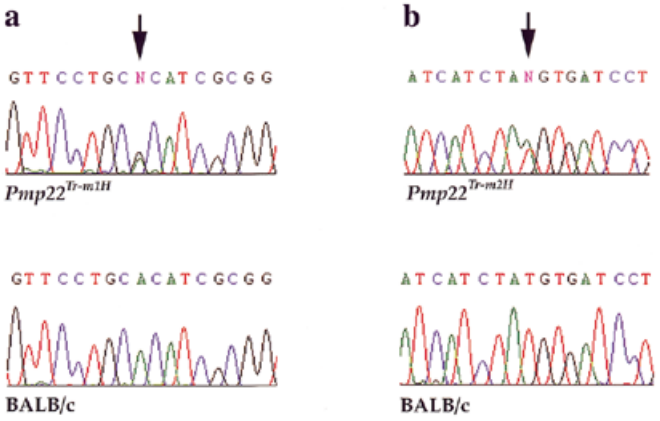

Figure 4. DNA sequence traces showing *Pmp22* point mutations in mutant progeny from Tr-m1H and Tr-m2H back-crosses to C3H/HeH. (**a**)Tr-m1H is heterozygous for an A→G transition (arrowed) in exon 2 resulting in a His→Arg amino acid substitution in the first transmembrane domain of the protein. (**b**) Tr-m2H is heterozygous for an A→T transversion (arrowed) in exon 5 resulting in a premature stop codon truncating Pmp22 by seven amino acids. Neither variant was detected in the BALB/c or C3H/HeH parental strains.

mutations is mirrored by both the *Pmp22* mouse mutants described here and previously described mutants.

Pmp22$^{Tr\text{-}m1H}$ causes a severe tremor phenotype with seizures, as does *Pmp22*^{Tr} (12). *Pmp22*$^{Tr\text{-}m2H}$ leads to a milder phenotype with less severe tremors and no seizures. *Pmp22*$^{Tr\text{-}J}$ results in a milder phenotype and pathology than *Pmp22*^{Tr} and lacks seizures (15) and *Pmp22*$^{Tr\text{-}Ncnp}$ is reported to produce a gait abnormality (14). The severe *Pmp22*^{Tr} and *Pmp22*$^{Tr\text{-}m1H}$ mutations affect the same amino acids altered in DSS (16), while the less severe *Pmp22*$^{Tr\text{-}J}$ mutation has been found in patients with CMT1A (17), indicating that the correlation between genotype and phenotype of *PMP22* mutations is well conserved between mice and humans. How this genotype–phenotype correlation relates to the function of PMP22 remains unclear.

The existence of Schwann cells in early myelin forms, as reported here and in the other trembler mutants (14,15) together with the delay of onset of myelination followed by severe demyelination in *Pmp22* deficient mice (18) suggests a role for Pmp22 in the initiation of myelination and myelin maintenance. Several studies have shown that *Pmp22*^{Tr}, *Pmp22*$^{Tr\text{-}J}$ and several CMT1A and DSS mutations impair trafficking of mutant PMP22 leading to its accumulation in intracellular compartments, resulting in failure to reach its normal location at the plasma membrane (19–22). HNPP, the least severe of the human neuropathies discussed here, can result from complete loss of one copy of *PMP22* (23) suggesting that *PMP22* haploinsufficiency can cause disease. As CMT1A frequently results from a duplication resulting in an additional copy of *PMP22* (24), PMP22 stoichiometric imbalance appears to be sufficient for pathogenesis, with excess PMP22 giving the more severe phenotype. It has been reported that PMP22 plays a structural role in the myelin membrane, where it binds peripheral myelin protein zero, a major constituent of peripheral nerve myelin (25); therefore an inappropriate level of PMP22 may result in loss of myelin membrane integrity and consequent neuropathy.

However, simple loss of function of one copy of *PMP22* cannot explain why a more severe phenotype can result from a point mutation of one *PMP22* allele than from complete loss of one copy of the *PMP22* gene. It has been suggested that mutant PMP22 can dimerize with wild-type PMP22 in intracellular compartments, sequestering both the mutant and wild-type forms and resulting in further loss of PMP22 at the plasma membrane (22); however, the evidence for this is contentious (19). Abnormal *PMP22* expression has also been shown to directly alter Schwann cell proliferation (26), adding to the complexity of the phenotype. To increase understanding of the relevance of Pmp22 sequestration in intracellular compartments to disease phenotype, we are currently determining the cellular localization of the Pmp22$^{Tr\text{-}m2H}$ mutant protein, which is truncated and gives a less severe phenotype than the missense mutations Pmp22^{Tr} and Pmp22$^{Tr\text{-}m1H}$.

Tr-m1H and Tr-m2H, which are the only *Pmp22* mutants exhibiting differing disease severities on a common genetic background, should help to further define the genotype–phenotype correlation of *Pmp22* mutants. By providing insights into the functional domains of Pmp22, these mutants may allow protein trafficking mechanisms and the binding of partners in the myelin membrane to be further dissected, thereby improving our understanding of the pathophysiological mechanism of peripheral neuropathy.

Tr-m1H and Tr-m2H are examples of disease-causing mutations identified from a large-scale mammalian mutagenesis programme. The identification and characterization of clinically relevant mutant phenotypes together with the identification of the underlying genetic lesion underlines the potential of phenotype-driven screens for the development of models of human disease. Moreover, the use of ENU mutagenesis for the generation of novel mouse mutants and eventually multiple mutations within a single gene, thereby increasing both the breadth and the depth of the mouse mutant resource, will be a major tool for systematic studies of mammalian gene function. However, the identification of the underlying genetic defect has undoubtedly been the largest bottleneck in phenotype-driven screens (27). Our rapid mapping strategy, which is optimized to scan several mutant mouse genomes at once, will go some way to reducing this bottleneck. In addition, we recently reported the use of IVF for the rapid generation of back-cross progeny for genetic mapping (6). These so-called ‘speed back-crosses’ enable the generation of large numbers of back-cross progeny for genotyping within 2 months. The use of speed back-crosses allied to rapid genotyping protocols of the type reported here will have a significant impact on throughput for mutant localization and move the bottleneck to candidate gene identification.

The rapid identification of mutations in *Pmp22* in Tr-m1H and Tr-m2H was facilitated by the presence of a promising candidate gene. Although the positional candidate approach is still not feasible in every case, the continuing characterization of the mouse genome through publicly supported mapping and sequencing projects will render it increasingly viable. In conclusion, the implementation of rapid gene identification protocols in conjunction with large-scale mutagenesis programmes is a powerful strategy. Utilizing this strategy in tandem with sensitive phenotype assessment, which allows the

identification of subtle phenotypes, should allow comprehensive functional analysis of a mammalian genome to become a reality.

MATERIALS AND METHODS

Animals

The animal studies described in this paper were carried out under the guidance issued by the Medical Research Council in *Responsibility in the Use of Animals for Medical Research* (July 1993) and Home Office Project Licence no. 30/1517. For mutagenesis, BALB/c males (Charles River, Margate, UK) were injected intraperitoneally with two doses of 100 mg/kg ENU (Sigma-Aldrich, Poole, UK) at ~10 weeks of age. Doses were separated by a 1 week period. Procedures for ENU administration, including detailed safety procedures, are described elsewhere (28). Phenotypic screens were carried out on F_1 progeny of mutagenized males mice crossed to C3H/He females (Charles River). Mating cages contained one male and up to two female occupants. Following weaning at 3 weeks of age, mice were housed in cages of about five mice. For inheritance testing, F_1 mice were back-crossed to the C3H/He strain and progeny classified for the phenotype identified in the founder. Mutant lines were subsequently maintained by back-crossing to C3H/He.

Phenotype assessment

The SHIRPA protocol was used to evaluate at least three Tr-m1H and Tr-m2H mice and three littermate controls. SHIRPA has been described previously (4) and at the website http://www.mgc.har.mrc.ac.uk/mutabase/shirpa_summary.html .

Histology

For brain and spinal cord histology, mice were given a lethal overdose of pentobarbitone, and intracardially perfused with 4% paraformaldehyde. Brain and spinal cord were removed and post-fixed in 4% paraformaldehyde overnight. Specimens were dehydrated through a series of alcohols, and embedded in paraffin wax. Sections (10 μm) were cut throughout the brain, and cervical and lumbar enlargements of the spinal cord. Sections were stained with cresyl violet, haematoxylin and eosin, and Luxol fast blue. For nerve histology, mice were intracardially perfused with 2% gluteraldehyde, 2% paraformaldehyde, and a section of the sciatic nerve removed and post-fixed in the same fixative overnight; or, mice were killed by cervical dislocation, and a portion of the sciatic nerve removed and immersion fixed in 2% gluteraldehyde, 2% paraformaldehyde for 2 h. All nerves were then post-fixed in 2% osmium tetroxide for 2 h, dehydrated through a series of alcohols, and embedded in araldite CY212. For light microscopy 1 μm semi-thin sections were cut, and stained with toludine blue. For electron microscopy 60–90 nm sections were cut, and stained with lead citrate and uranyl acetate.

Linkage analysis

Tail snips were taken from 45 Tr-m1H and 44 Tr-m2H mutant back-cross mice and DNA extracted using standard procedures. DNA concentrations were measured by UV absorbance and equimolar aliquots of DNA combined for each strain. The DNA pools, together with DNA from BALB/c, C3H/HeH and F_1 mice, were screened with 229 simple tandem repeat markers polymorphic between BALB/c and C3H/HeH selected from the 410 marker set available from Research Genetics (Huntsville, AL), and arranged into 22 panels. Genotyping was performed using a PE Biosystems 377 PRISM system (Foster City, CA) in accordance with the manufacturer's instructions. Genotype data were analysed using a modified version of TrueAllele software (Cybergenetics, Pittsburgh, PA).

Determination of *Pmp22* genomic structure

PCR primers 5′-cactatgggtgacccagtc-3′ and 5′-cgtgtggccccagtgctggc-3′, derived from the 3′ untranslated region of *Pmp22*, were used to identify clone 201-C-16 from a mouse BAC genomic library (Research Genetics). PCR conditions were as follows: 20 μl reactions containing 200 μM dNTPs, 1.5 mM $MgCl_2$, 1 U of *Taq* platinum (PE Biosystems) together with the supplied buffer and the recommended amount of template were subjected to 35 cycles of 94°C for 30s, 65°C for 30s and 72°C for 30s. The product (169 bp) was identified by electrophoresis in a 2% agarose gel. A 250 ml culture of 201-C-16 was grown overnight and DNA prepared using a Qiagen plasmid maxi kit. Direct sequencing of the BAC clone DNA to determine intron–exon boundaries was performed using the protocol described at http://www.tree.caltech.edu/protocols/BAC_end_sequencing.html . Primers used for sequencing were: 5′-ctgcacatcgcggtgctagtgttgc-3′ and 5′-gtacagttctgccagagatcagtcg-3′ (intron B), 5′-cgccttgggagccgtccaacactgc-3′ and 5′-gaagatgacagacaggatcatggtggc-3′ (intron C) and 5′-ccaaaggcggccggttttacatcactgg-3′ and 5′-ctgtgcctcactgtgtagatggccgc-3′ (intron D).

Pmp22 mutation analysis

Flanking intronic and untranslated sequences were used to design primers for amplification of exons 2–5 from Tr-m1H, Tr-m2H, BALB/c and C3H/HeH and subsequent sequence analysis. Primer sequences were: 5′-gcaccgctcctctgatcccgagc-3′ and gcactggctgggaacccagagc-3′ (exon 2), 5′-ggaataccatccttt-gccctgc-3′ and 5′-cccagttaggaccaatctgc-3′ (exon 3), 5′-ggcag-gtcctcctggccattcc-3′ and 5′-gcaggaatgaattgttttcccc-3′ (exon 4) and 5′-ggaggctcagacacatcttcc-3′ and 5′-cctgtggaccctatgcgcgc-3′ (exon 5). PCR reaction conditions were as described above, using 30 ng of genomic DNA as template. PCR products were purified using Qiagen QIAquick columns and sequenced directly using an Applied Biosystems 377 PRISM system in accordance with the manufacturer's instructions.

ACKNOWLEDGEMENTS

We thank Lesley Rooke and Colin Clapham for technical assistance and See-Kiong Ng for assistance with software. This work was supported by SmithKline Beecham Pharmaceuticals and the Medical Research Council.

REFERENCES

1. Nolan, P., Peters, J., Strivens, M., Rogers, D., Hagan, J., Spurr, N., Gray, I.C., Vizor, L., Brooker, D., Whitehill, D. *et al.* (2000) A systematic genome-wide phenotype-driven mutagenesis programme for gene function studies in the mouse. *Nature Genet.*, in press.

2. Russell, W.L., Kelly, E.M., Hunsicker, P.R., Bangham, J.W., Maddux, S.C. and Phipps, E.L. (1979) Specific-locus test shows ethylnitrosourea to be the most potent mutagen in the mouse. *Proc. Natl Acad. Sci. USA*, **76**, 5818–5819.
3. Rogers, D.C., Fisher, E.M., Brown, S.D., Peters, J., Hunter, A.J. and Martin, J.E. (1997) Behavioral and functional analysis of mouse phenotype: SHIRPA, a proposed protocol for comprehensive phenotype assessment. *Mamm. Genome*, **8**, 711–713.
4. Nelis, E., Haites, N. and Van Broeckhoven, C. (1999) Mutations in the peripheral myelin genes and associated genes in inherited peripheral neuropathies. *Hum. Mutat.*, **13**, 11–28.
5. Jones, B.J. and Roberts, D.J. (1968) The quantitative measurement of motor inco-ordination in naive mice using an accelerating rotarod. *J. Pharm. Pharmacol.*, **20**, 302–304.
6. Thornton, C.E., Brown S.D.M. and Glenister P.H. (1999) Large numbers of mice established by in vitro fertilisation with cryopreserved spermatazoa: implications and applications for genetic resource banks, mutagenesis screens and mouse back-crosses. *Mamm. Genome*, **10**, 987–992.
7. Perlin, M.W., Lancia, G. and Ng, S.-K. (1995) Toward fully automated genotyping: genotyping microsatellite markers by deconvolution. *Am. J. Hum. Genet.*, **57**, 1199–1210.
8. Whitehead Institute for Biomedical Research/MIT Center for Genome Research (http://www-genome.wi.mit.edu/).
9. Mouse Genome Database (MGD), Mouse Genome Informatics, The Jackson Laboratory, Bar Harbor, ME (http://www.informatics.jax.org/).
10. Roa, B.B., Garcia, C.A., Suter, U., Kulpa, D.A., Wise, C.A., Mueller, J., Welcher, A.A., Snipes, G.J., Shooter, E.M., Patel, P.I. *et al*. (1993) Charcot-Marie-Tooth disease type 1A. Association with a spontaneous point mutation in the PMP22 gene. *N. Engl. J. Med.*, **329**, 96–101.
11. Valentijn, L.J., Ouvrier, R.A. van den Bosch, N.H., Bolhuis, P.A., Baas, F. and Nicholson, G.A. (1995) Dejerine-Sottas neuropathy is associated with a de novo PMP22 mutation. *Hum. Mutat.*, **5**, 76–80.
12. Suter, U., Welcher, A.A., Ozcelik, T., Snipes, G.J., Kosaras, B., Francke, U., Billings-Gagliardi, S., Sidman, R.L. and Shooter, E.M. (1992) Trembler mouse carries a point mutation in a myelin gene. *Nature*, **356**, 241–244.
13. Suter, U., Moskow, J.J., Welcher, A.A., Snipes, G.J., Kosaras, B., Sidman, R.L., Buchberg, A.M. and Shooter, E.M. (1992) A leucine-to-proline mutation in the putative first transmembrane domain of the 22-kDa peripheral myelin protein in the trembler-J mouse. *Proc. Natl Acad. Sci. USA*, **89**, 4382–4386.
14. Suh, J.G., Ichihara, N., Saigoh, K., Nakabayashi, O., Yamanishi, T., Tanaka, K., Wada, K. and Kikuchi, T. (1997) An in-frame deletion in peripheral myelin protein-22 gene causes hypomyelination and cell death of the Schwann cells in the new Trembler mutant mice. *Neuroscience*, **79**, 735–744.
15. Henry, E.W., Cowen, J.S. and Sidman, R.L. (1983) Comparison of Trembler and Trembler-J mouse phenotypes: varying severity of peripheral hypomyelination. *J. Neuropathol. Exp. Neurol.*, **42**, 688–706.
16. Ionasescu, V.V., Searby, C.C., Ionasescu, R., Chatkupt, S., Patel, N. and Koenigsberger, R (1997) Dejerine-Sottas neuropathy in mother and son with same point mutation of PMP22 gene. *Muscle Nerve*, **20**, 97–99.
17. Valentijn, L.J., Baas, F., Wolterman, R.A., Hoogendijk, J.E., van den Bosch, N.H., Zorn, I., Gabreels-Festen, A.W., de Visser, M. and Bolhuis, P.A. (1992) Identical point mutations of PMP-22 in Trembler-J mouse and Charcot-Marie-Tooth disease type 1A. *Nature Genet.*, **2**, 288–291.
18. Adlkofer, K., Martini, R., Aguzzi, A., Zielasek, J., Toyka, K.V. and Suter, U. (1995) Hypermyelination and demyelinating peripheral neuropathy in Pmp22-deficient mice. *Nature Genet.*, **11**, 274–280.
19. D'Urso, D., Prior, R., Greiner-Petter, R., Gabreels-Festen, A.A. and Muller, H.W. (1998) Overloaded endoplasmic reticulum-Golgi compartments, a possible pathomechanism of peripheral neuropathies caused by mutations of the peripheral myelin protein PMP22. *J. Neurosci.*, **18**, 731–740.
20. Naef, R., Adlkofer, K., Lescher, B. and Suter, U. (1997) Aberrant protein trafficking in Trembler suggests a disease mechanism for hereditary human peripheral neuropathies. *Mol. Cell. Neurosci.*, **9**, 13–25.
21. Naef, R. and Suter, U. (1999) Impaired intracellular trafficking is a common disease mechanism of PMP22 point mutations in peripheral neuropathies. *Neurobiol. Dis.*, **6**, 1–14.
22. Tobler, A.R., Notterpek, L., Naef, R., Taylor, V., Suter, U. and Shooter E.M. (1999) Transport of Trembler-J mutant peripheral myelin protein 22 is blocked in the intermediate compartment and affects the transport of the wild-type protein by direct interaction. *J. Neurosci.*, **19**, 2027–2036.
23. Chance, P.F., Alderson, M.K., Leppig, K.A., Lensch, M.W., Matsunami, N., Smith, B., Swanson, P.D., Odelberg, S.J., Disteche, C.M. and Bird, T.D. (1993) DNA deletion associated with hereditary neuropathy with liability to pressure palsies. *Cell*, **72**, 143–151.
24. Patel, P.I., Roa, B.B., Welcher, A.A., Schoener-Scott, R., Trask, B.J., Pentao, L., Snipes, G.J., Garcia, C.A., Francke, U., Shooter, E.M. *et. al*. (1992) The gene for the peripheral myelin protein PMP-22 is a candidate for Charcot-Marie-Tooth disease type 1A. *Nature Genet.*, **1**, 159–165.
25. D'Urso, D., Ehrhardt, P. and Muller, H.W. (1999) Peripheral myelin protein 22 and protein zero: a novel association in peripheral nervous system myelin. *J. Neurosci.*, **19**, 3396–3403.
26. Zoidl, G., Blass-Kampmann, S., D'Urso, D., Schmalenbach, C. and Muller, H.W. (1995) Retroviral-mediated gene transfer of the peripheral myelin protein PMP22 in Schwann cells: modulation of cell growth. *EMBO J.*, **14**, 1122–1128.
27. Justice, M.J., Noveroske, J.K., Weber, J.S., Zheng, B. and Bradley, A. (1999) Mouse ENU mutagenesis. *Hum. Mol. Genet.*, **8**, 1955–1965.
28. Nolan, P.M., Kapfhamer, D. and Bucan, M. (1997) Random mutagenesis screen for dominant behavioral mutations in mice. *Methods*, **13**, 379–395.